Title

Sugarcane bagasse derived phosphorylated cellulose as substrates for potassium release induced by phosphates surface and drying methods

Authors

Messa, Lucas Luiz
Hsieh, You-Lo
Faez, Roselena

Publication Date

2022-11-01

DOI

10.1016/j.indcrop.2022.115350

Industrial Crops & Products 187 (2022) 115350

Contents lists available at ScienceDirect

Industrial Crops & Products

journal homepage: www.elsevier.com/locate/indcrop

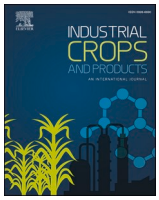

Sugarcane bagasse derived phosphorylated cellulose as substrates for potassium release induced by phosphates surface and drying methods

Lucas Luiz Messa [a,b], You-Lo Hsieh [c], Roselena Faez [a,b,*]

[a] Laboratory of Polymeric Materials and Biosorbents, Federal University of São Carlos, UFSCar, 13600970 Araras, São Paulo, Brazil
[b] Graduate Program in Materials Science and Engineering, University of Sao Paulo, Pirassununga, São Paulo 13635900, Brazil
[c] Biological and Agricultural Engineering, University of California, Davis, CA 95616, United States

ARTICLE INFO

Keywords:
Agricultural residue
Controlled-release fertilizer
Phosphorylation

ABSTRACT

Encapsulation and controlled release of potassium by phosphorylated cellulose (P-cell) was systematically demonstrated by drying of aqueous P-cell suspensions with potassium chloride (KCl) in varied stoichiometric K^+/Cell-O-HPO_3 ratios of 1:1, 2:1, and 4:1, and dried into powder-like fibrous fluffs, paper-like films, and three-dimensional porous structures by spray-, oven-, and freeze-drying. Cellulose isolated from sugarcane bagasse as agricultural waste was optimally phosphorylated at 1:0.5:2 anhydroglucose (AHG)/$(NH_4)_2HPO_4$/$CO(NH_2)_2$ as 14.6 μm wide, *ca.* 366 μm long, highly crystalline (72%) microfibers with 2.4 mmol g^{-1} charge. Oven drying led to more crystalline (73%) and thermally stable (252.1 °C) films than spray-dried powders (67%, 250.5 °C) and freeze-dried porous bulk (71%, 249.8 °C). The release of highly water-soluble KCl from these three P-cell substrates was highest from the fibrous (90.4–97.3%), three-dimensional porous structure solids (73.5–81.7%), then films (60.4–74.5%), thus could be tuned by varying the anionic/cationic loadings along with drying methods.

1. Introduction

Sugarcane (*Saccharum officinarum*) is the most cultivated crop in the world, with 1.84 billion tonnes produced in the 2017/2018 harvest. Brazil produces 40% sugarcane, with over 747 million tonnes processed mainly into sugar or alcohol (FAOSTAT, 2020). Sugarcane processing is responsible for generating 30% bagasse residue, *e.g.*, 195 million tonnes (Ferreira-Leitao et al., 2010), and thus this is the most agricultural biomass in Brazilian agriculture. Furthermore, bagasse stands out as an attractive cellulose source for different applications as a readily available waste with a relatively high cellulose content of approximately 42% (Rocha et al., 2015).

Cellulose, the most abundant polymer, is synthesized by plants and bacteria and has been commonly used in its native fibrous forms in packaging, paper, and textile production (Abushammala and Mao, 2019). The linear syndiotactically arranged D-anhydroglucopyranose units linked by β-(1→4)-glycosidic bonds (Kim et al., 2006) is fibrillar, semicrystalline (Saxena and Brown, 2005), and hydrophilic (Cichosz and Masek, 2019). In addition, the intrinsic characteristics of biodegradability (Vikman et al., 2015), renewability at relatively low cost (Ardanuy et al., 2015), and versatile chemical reactivity (Vuoti et al., 2013) have made desirable cellulose material for many additional potential applications. However, the high hydrophilicity (Rol et al., 2019a) and low thermal resistance (Korovnikova et al., 2020) are limiting factors for certain applications.

Cellulose derivatives are particularly interesting due to their new properties beyond the original cellulose. Among the most prominent are phosphorylated cellulose derivatives produced by the chemical phosphorylation method using a greener condition in a water-based urea system with inorganic phosphate salts (Ghanadpour et al., 2015; Messa et al., 2021; Naderi et al., 2016; Noguchi et al., 2017). Phosphorylation with diammonium hydrogen phosphate ($(NH_4)_2HPO_4$) in the presence of urea ($(NH_2)_2CO$) introduces negatively charged phosphoric groups through the esterification of cellulose hydroxyls (Messa et al., 2021) while minimizing fiber dissolution (Ghanadpour et al., 2015). These phosphorylated cellulose derivatives have been demonstrated to be excellent flame-retardant materials (Ghanadpour et al., 2018b, 2015), highly fire-protecting coating (Ghanadpour et al., 2018a), bio-adsorbents for selective adsorption (Lehtonen et al., 2020; Liu et al., 2015; Mautner et al., 2016), and composites for bone tissue engineering materials (Li et al., 2012). However, the use of phosphorylated cellulose derivatives as a substrate for chemical delivery is lacking. Incorporating phosphorus moieties *via* phosphorylation of cellulose offers ample surface anionic charges to allow binding the cationic ions of macro- and

* Corresponding author at: Laboratory of Polymeric Materials and Biosorbents, Federal University of São Carlos, UFSCar, 13600970 Araras, São Paulo, Brazil.
E-mail address: faez@ufscar.br (R. Faez).

https://doi.org/10.1016/j.indcrop.2022.115350
Received 9 February 2022; Received in revised form 4 July 2022; Accepted 8 July 2022

micronutrients for potential controlled delivery of plant nutrition.

The capability to retard or control plant nitrogen, phosphorous, and potassium macronutrients from varied fertilizer sources, *i.e.,* urea ($(NH_2)_2CO$), potassium sulfate (K_2SO_4), diammonium hydrogen phosphate ($(NH_4)_2HPO_4$), dipotassium hydrogen phosphate (K_2HPO_4), over a prolonged time interval can also minimize environmental pollution from nutrient loss (Chen et al., 2018). The enhanced efficiency fertilizers (EEFs) based on cellulose or its derivatives have been predominantly reported as hydrogels (Bortolin et al., 2013; Kenawy et al., 2018; Li et al., 2015; Mohammadi-Khoo et al., 2016; Muharam et al., 2020; Olad et al., 2018; Rop et al., 2018; Senna et al., 2015; Zhang et al., 2020). For instance, the grafting copolymerization of sawdust cellulose, acrylic acid, acrylamide, and urea was performed using N, N′-methylenebis as crosslinker and potassium persulfate as an initiator to synthesize hydrogel fertilizers for slow-release of urea achieving 82.4% of release in water for 8 h (Zhang et al., 2020). Crosslinking bromoacetylated cellulose with urea in the presence of N, N-dimethylacetamide, and triethylamine was conducted to form hydrogels that displayed a significantly slowed urea release of 97% in 720 h in water (Mohammadi-Khoo et al., 2016). Furthermore, only a few have reported cellulose-based EEFs in forms other than hydrogels. Solution-casting of emulsions based on ethylcellulose, vinyl acetate, butyl acrylate, and urea has been performed to obtain films for slow nitrogen release, *i.e.,* 84.1% after 42 days in water (Li et al., 2018). Most recently, double-coating urea having ethylcellulose as an inner layer and cellulose-based superabsorbent (pretreated cellulose grafted with acrylic acid and acrylamide) as outer layer slowed nitrogen release in soil to 58.6% within 15 days (Zhang and Yang, 2020). However, most of these cellulose-based EEFs require extra chemicals (*i.e.*, synthetic polymers, crosslinkers, polymerization initiators, and organic solvents), or the processes are complex and expensive for agricultural applications. Therefore, there is a clear need to explore facile and greener routes to generate cellulose-based EEFs with no or minimum additional chemicals.

In this work, aqueous suspensions of 14.6 μm (± 5.2 μm, N = 87) wide and 365.9 (± 164.7 μm, N = 56) long phosphorylated cellulose (P-cell) fibers with 2.4 ± 0.4 mmol g^{-1} charge were incorporated with counterion salt (potassium chloride) and then dried into different solid forms of powder-like fibrous, paper-like films, and three-dimensional porous structures. The highly water-soluble potassium chlorite was incorporated at 1, 2, and 4:1 K^+/Cell-O-HPO_3^- molar ratios to discern the effects of attractive electrostatic forces in these solid forms on their release properties. Also, we evaluate the effects of drying methods, *i.e.*, spray-, oven-, and freeze-drying, on the structure, morphology, crystallinity, and thermal stabilities of these solids. For agriculture crops, potassium chloride is the most extensively used source of potassium fertilizer (Kafkafi et al., 2001), an essential nutrient for the growth and development of plants. Thus, the prolonged release of potassium is particularly interesting to avoid loss during fertilization. The highly water-soluble potassium chlorite was also used as a model counterions for the *in-water* release capacity study.

2. Material and methods

2.1. Materials

Cellulose was isolated from sugarcane bagasse by a two-step 1.4% $NaClO_2$ (pH 3.5, 70 °C, 5 h) and 5% KOH (room temperature for 24 h, then 90 °C for 2 h) process to a 42% yield (Messa et al., 2021). Diammonium hydrogen phosphate ($(NH_4)_2HPO_4$, ACS reagent grade, 99%) and urea ($(NH_2)_2CO$, ACS reagent grade, 99%) were purchased from Dinâmica Química Contemporânea (Brazil) and used for cellulose phosphorylation. Potassium chloride (KCl, 99%, Synth-Brazil), glacial acetic acid (CH_3COOH, 99%, J. T. Baker-Brazil), and sodium hydroxide (NaOH, 88%, Synth-Brazil) were used as received. Water used was from Milli-Q plus water purification system (Millipore Corporate, Billerica, MA).

2.2. Phosphorylation of sugarcane bagasse cellulose

Phosphorylation of cellulose was conducted following a previously reported procedure (Messa et al., 2021). Cellulose was impregnated with $(NH_4)_2HPO_4$ at 0.5:1 $(NH_4)_2HPO_4$/anhydroglucose unit (AHG) molar ratio in moderate stoichiometric excess of the *ca.* 31% amorphous cellulose, to which 2 mol of urea was added and stirred at RT for 30 min, then dried at 40 °C, followed by curing at 150 °C for 30 min. The reacted cellulose was washed with water until the conductivity was lowered to < 5 μS cm^{-1} to remove weakly attached chemicals, filtered to recover the light-yellow color phosphorylated cellulose (P-cell), and stored under vacuum for further characterizations.

2.3. Drying of KCl loaded P-cell suspensions via spray-drying (SD), freeze-drying (FD), and oven-drying (OD)

P-cell fibers were transferred to water to form 1.0 w/v% suspensions and homogenized for 5 min using an ultra turrax disperser (15.000 rpm, IKA T 25 digital). The suspensions were loaded with KCl at 1, 2, and 4:1 K^+/Cell-O-HPO_3^- molar ratios, corresponding to respective 0.0025, 0.0051, 0.0102 mol KCl under constant stirring for 30 min, and dried in three different ways: rapid spray-dried in hot air, freezing in a freezer, then freeze-dried, and slow oven-dried. KCl-loaded P-cell suspensions (100 mL) were spray-dried using a laboratory scale spray dryer (B-290, Buchi Corp., Switzerland) coupled with a 1.5 mm two-fluid atomization system at 180 °C inlet temperature, 20% suspension-feeding rate, and 473 L h^{-1} drying air stream. In freeze-drying, KCl-loaded P-cell suspensions (10 mL) were first transferred to 15 mL polypropylene conical tubes and frozen at −80 °C for 15 h, then lyophilized (−47 °C, < 100 μHg vacuum) for 2 days in a freeze-drier (L101, Liotop). Oven-drying of KCl-loaded P-cell suspensions (10 mL) in polypropylene weighing boats was performed at 40 °C for 8 h. All dried solids were stored under a vacuum for further characterization. The dried P-cell and P-cell/KCl solids were denoted by the drying methods of spray-drying (SD), freeze-drying (FD), or oven-drying (OD) followed by the cationic-anionic molar ratio, *i.e.*, 1:1, 1:2, or 1:4.

2.4. Characterization of aqueous phosphorylated cellulose suspensions

2.4.1. Optical light microscopy

0.1 w/v% P-cell aqueous suspensions were observed using a Leica DM4000B optical microscope. The width (N = 87) and length (N = 56) of fibers were measured using an image analyzer (ImageJ, NIH, USA), and the average value, standard deviation, and distribution were derived using OriginLab Pro 2016.

2.4.2. Conductometric titration

The total charge on P-cell fibers was determined by conductometric titration of 50 mL P-cell suspension at 0.025 wt% with 0.01 M NaOH. Before titration, the suspension's pH and electrical conductivity were controlled by adding the appropriate amount of 1 M HCl and 0.5 M NaCl. GEHAKA CG 2000 conductivity meter was used to record the conductivity values of P-cell suspensions. The total charge (σ) was calculated from Eq. 1 (Jiang et al., 2013), in which m is P-cell mass (g), c is NaOH concentration (M), and v_1 and v_2 are the volumes (mL) of NaOH consumed for neutralization of phosphate acids on P-cell. In addition, the average and standard deviation values from the three measurements were reported.

$$\sigma = \frac{cv}{m} = \frac{c(v_1 - v_2)}{m} \quad \text{Eq. 1}$$

2.4.3. Drying yield and productivity

The drying yield (%) from FD, SD, and OD was calculated based on the weighed mass of solid collected after drying and the initial weight of solids in each suspension. In spray-drying, solids accumulated on the

inside wall of the cyclone were not considered for yield determination.

$$\text{Drying Yield}(\%) = \frac{\text{Weight after drying (g)}}{\text{Solids content weight in suspension (g)}} \text{x100} \quad (2)$$

The productivity (g h^{-1}) of drying methods was calculated from the weighed mass of solid collected after drying and the drying time (h) by the previously reported method (Nardi et al., 2020).

$$\text{Productivity}\left(gh^{-1}\right) = \frac{\text{Weight after drying (g)}}{\text{Drying time } \left(h^{-1}\right)} \quad (3)$$

2.5. Solid-state characterization of SCB cellulose, P-cell, and all FD, SD, and OD P-cell/KCl

2.5.1. Fourier transform infrared spectroscopy (FTIR)

FTIR spectra of samples in KBr pellets (1:100 w/w) were collected using a Bomem MB-100 spectrometer in transmittance mode from an accumulation of 128 scans at 4 cm^{-1} over 4000–400 cm^{-1} region under ambient conditions.

2.5.2. Thermogravimetric analysis (TGA)

TGA of each sample (*ca.* 5–10 mg) was conducted at 10 °C min^{-1} heating rate from 25 °C to 700 °C under flowing nitrogen (50 mL min^{-1}) on TGA 4000 Thermogravimetric Analyzer (PerkinElmer, EUA). Derivative thermogravimetric curve (dTGA) was the first derivative from the TGA data.

2.5.3. X-ray diffraction (XRD)

XRD samples were prepared by compressing them on a glass slide by hand, and their XRD spectra were collected on a Rigaku MiniFlex 600 powder diffractometer using a Cu Kα radiation (= 1.5406 Å) generated at 45 kV and 40 mA at 10° min^{-1} rate from 10° to 45° 2θ. The crystallinity index (CrI) of samples was determined using Eq. 4 (Segal et al., 1959) from the intensity of 200 peaks (2θ = 22.6°), denoted as I_{200}, and the minimum intensity between 200 and 110 peaks (2θ = 18.7°), designated as I_{am}.

$$\text{CrI}(\%) = \frac{I_{200} - I_{am}}{I_{200}} \quad (4)$$

2.5.4. Scanning electron microscopy (SEM)

SEM samples were prepared by mounting them with conductive carbon tape, followed by sputter-coating with gold, and then examined by a field-emission scanning electron microscopy (JSM7500F, JEOL) at a 4–8 mm working distance and 2-kV accelerating voltage. The fracture morphology was performed from cryosectioned in the transversal direction. The elemental analysis was conducted using an EDS detector (UltraDry, Thermo Fisher Scientific) coupled to SEM with 10 kV accelerating voltage at 500x magnification.

2.5.5. In-water potassium release capacity

The ability of the spray-, freeze-, and oven-dried solids to release potassium was investigated using SD, FD, and OD P-cell/KCl samples loaded with increasing KCl molar mass (0.0025, 0.0051, and 0.0102) to relate the effects of surface anionic charges on potassium counterion binding to fibers and their solid structure on KCl encapsulating. The *in*-water release of potassium from SD, FD, and OD P-cell/KCl samples (*ca.* 100 mg) was monitored by placing each into a polypropylene nonwoven sachet (7 × 5 cm) immersed in 50 mL deionized water under ambient conditions and without stirring. The aqueous solution was sampled at predetermined time intervals to quantify the potassium concentration using flame photometric (Digimed, DM 62) based on the calibration curve determined using aq. KCl (5, 10, 20, 30, 40, 50, 60, 70, and 80 mg L^{-1}) and the sachet were transferred to another fresh 50 mL of deionized water. The average value and standard deviation of potassium release were obtained from three measurements and reported.

2.5.6. Potassium release mechanism and kinetics

The mechanism and parameters kinetics of the first 60% potassium release from dried P-cell/KCl solids were investigated using the Korsmeyer-Peppas model (Eq. 5) (Korsmeyer et al., 1983), which is commonly applied to predict the release of drugs from the polymeric materials,

$$\frac{M_t}{M_\infty} = \text{k}t^n \quad (5)$$

where $Mt/M\infty$ is the fraction of potassium released at time *t*. The release system characteristic is defined as *k*, and *n* is the exponent of diffusion of the release mechanism.

3. Results and discussion

3.1. Characterization of phosphorylated SCB cellulose

The isolated SCB cellulose was phosphorylated at 0.5 mol $(NH_4)_2HPO_4$ and 2 mol $CO(NH_2)_2$ equivalent of AHG in the non-crystalline cellulose at 150 °C for 30 min to produce phosphorylated cellulose (P-cell) (Fig. S1). Reaction from 1:0.5:2 AHG/$(NH_4)_2HPO_4$/$CO(NH_2)_2$ turned the white cellulose to light-yellow P-cell, manifesting that the phosphorylation occurred for SCB cellulose, as previously observed (Rol et al., 2019b). Furthermore, the optical microscopy of homogenized suspension *via* turrax (Fig. 1a) revealed P-cell to be mainly in the form of 14.6 ± 5.2 μm wide and 365.9 ± 164.7 μm long microfibers (Fig. 1b-d). This observation is expected and consistent with unchanged fiber morphology from phosphorylation of bleached eucalyptus kraft pulp even under much harsher conditions (1/1.2/4.9 molar ratio at 150 °C for 1 h) (Rol et al., 2019b).

Reacting SCB cellulose with $(NH_4)_2HPO_4$ involves esterification of the hydroxyl groups to yield cellulose phosphate (Cellulose-O-P(=O)$(OH)_2$) (Messa et al., 2021). All phosphoric groups were first converted to their protonated form with added HCl before the conductimetric titration of aqueous P-cell suspensions (Fig. 2a). During conductimetric titration, an initial decrease in conductivity is due to the neutralization of free acid by the base titrant. Then a plateau region is attained, signifying the consumption of protons from surface phosphate acids followed by a rapid increase due to the excess NaOH. The charge of the P-cell was determined by the amount of NaOH titrant at the plateau region and calculated to be 2.4 ± 0.4 mmol per gram of SCB cellulose. In comparison, a lower 1.84 μeq g^{-1} charged fibers were synthesized from sulfite softwood pulp with five times higher $(NH_4)_2HPO_4$ and urea at 1/2.5/10 before filtering step dried and cured at 150 °C for 30 min (Ghanadpour et al., 2015). Slightly higher 2.93 mmol g^{-1} charges were produced from hardwood (eucalyptus) kraft pulp using two times of $(NH_4)_2HPO_4$ and urea or 1/1.2/4.9 AHG/$(NH_4)_2HPO_4$/urea ratio at 150 °C for 1 h (Rol et al., 2019b). A slightly lower 2.20 mmol g^{-1} charged phosphorylated pulp was reported on softwood pulp employing slightly higher $NH_4H_2PO_4$ and urea (1/0.6/3.2 molar ratio) at 165 °C for 10 min (Noguchi et al., 2017). Therefore, this optimized phosphorylation (1:0.5:2 AHG/$(NH_4)_2HPO_4$/$CO(NH_2)_2$, 150 °C, 30 min) of SCB cellulose produced similar or higher charged P-cell (2.4 ± 0.4 mmol g^{-1}) compared to phosphorylation of various pulp cellulose but with much less $(NH_4)_2HPO_4$ and urea and one less filtering step.

FTIR spectra showed the chemical changes of SCB cellulose following phosphorylation (Fig. 2b). The broad O-H stretching band at 3400 cm^{-1}, C-H stretching bands and C-O bending at 2900 and 1060 cm^{-1}, and the glycosidic C-H deformation at 897 cm^{-1} were retained throughout (Kumar et al., 2014; Mandal and Chakrabarty, 2011; Wulandari et al., 2016). 1718 cm^{-1} band of C═O stretching (Aoki and Nishio, 2010) is due to oxidation in cellulose phosphorylation. The slight P═O and P-OH stretching bands (Aoki and Nishio, 2010) at 1205 and 928 cm^{-1} of P-cell

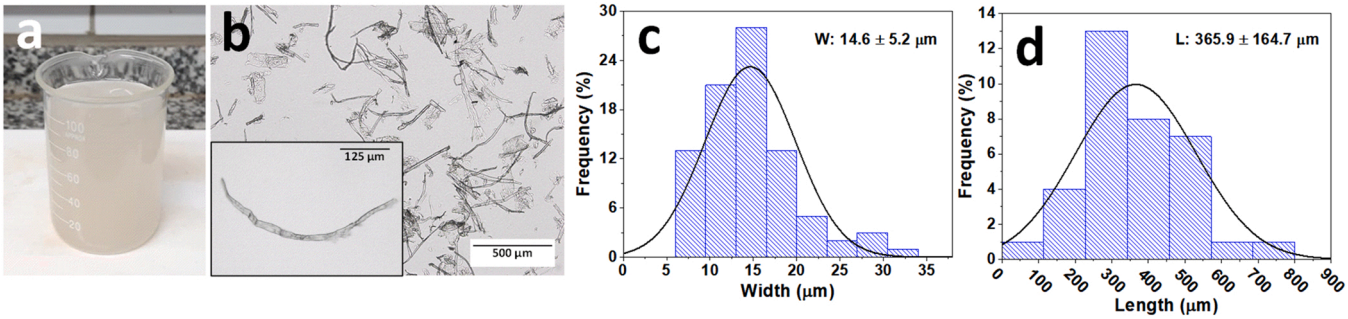

Fig. 1. Phosphorylated cellulose with 1:0.5:2 AHG/$(NH_4)_2HPO_4$/$CO(NH_2)_2$ at 150 °C for 30 min: (a) image of 1.0 w/v% homogenized suspension *via* turrax, (b) optical microscopy images, and (c, d) fiber widths, lengths, and their distributions.

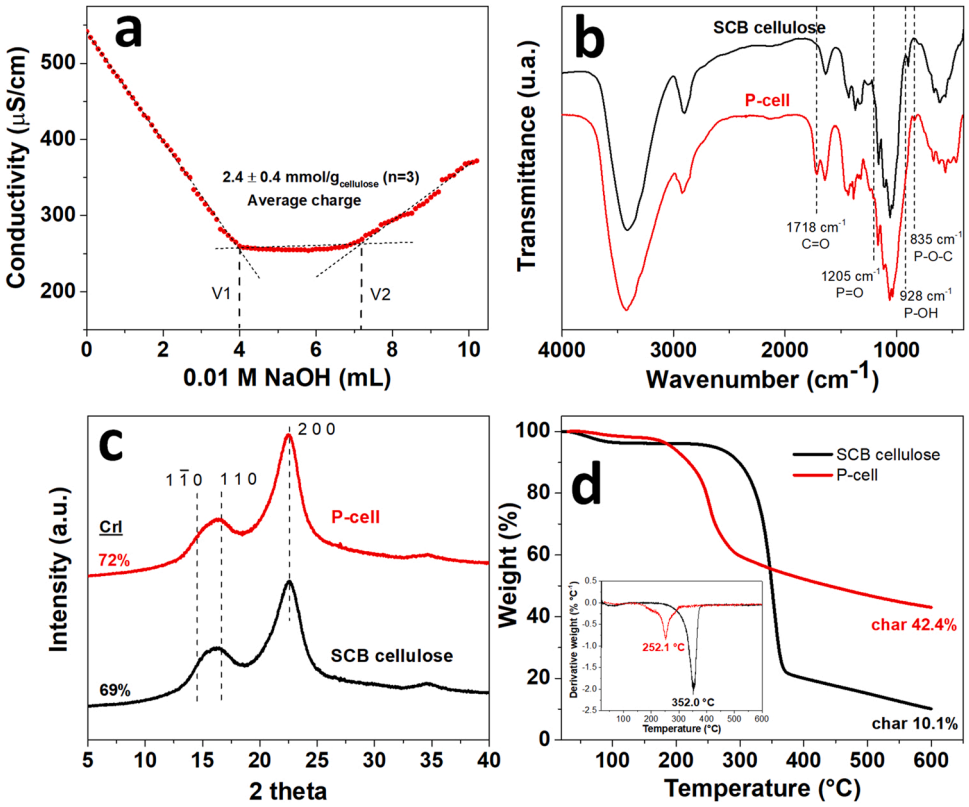

Fig. 2. Characterization of P-cell (red) and SCB cellulose (black): (a) total charge by conductimetric titration, (b) FTIR spectra, (c) XRD patterns, and (d) TGA and dTGA curves.

and the more distinct 835 cm^{-1} P-O-C aliphatic bonds (Suflet et al., 2006) support the phosphate groups incorporation into cellulose structure.

P-cell samples had similar XRD patterns as SCB cellulose with diffraction peaks at $2\theta = 14.6°$, 16.7°, 22.7° corresponding to the 1 1̄ 0, 1 1 0, and 2 0 0 crystallographic planes in a monoclinic lattice, confirming the Iβ crystalline structure of cellulose to be maintained following phosphorylation and homogenization (Fig. 2c). Furthermore, the crystallinity index (CrI) for P-cell (72%) was slightly higher than SCB cellulose (69%), suggesting loss of amorphous cellulose due to dissolution. Similarly, no changes in the crystal structure and constant crystallinity indices values (84–86% range) of phosphorylated derivatives at varying charges from 0.0 to 2.2 mmol g^{-1} were reported from phosphorylation of softwood pulp with $NH_4H_2PO_4$ and urea (1/0.6/3.2) (Noguchi et al., 2017). Essentially, the conversion of surface hydroxyl groups to phosphate groups during $(NH_4)_2HPO_4$ phosphorylation was evident from the FTIR, while the cellulose core remained as Iβ crystalline structure.

Cellulose was thermally stable up to 265 °C, showing a T_{max} at 352.0 °C to coincide with an expressive 75% mass loss and leaving 10.1% char at 600 °C (Fig. 2d). On the other hand, P-cell exhibited decreased thermal stability that started below 200 °C and a significantly lower T_{max} of 252.1 °C. As a result, P-cell lost nearly 39% of its mass but left a massively higher 42.4% char at 600 °C. The deteriorated thermal stability is associated with solid-to-gas phase transitions from dephosphorylation of the phosphoric groups on phosphorylated cellulose (Shi et al., 2015), providing evidence for phosphorylation. Similarly, phosphorylated microcrystalline celluloses from P_2O_5/H_3PO_4/triethyl phosphate/hexanol oxidative phosphorylation had similar decreased thermal decomposition from 338.4 °C (T_{max}) to 206.9–229.3 °C and an increased char to 36.6–37.1% (Niu et al., 2020).

3.2. Drying P-cell/KCl suspensions via spray-drying (SD), freeze-drying (FD), and oven-drying (OD)

KCl was incorporated with aqueous P-cell at 1, 2, and 4:1 K^+/Cell-O-HPO_3^- molar ratios and dried into SD, FD, and OD solids (Fig. S2a). Spray drying of 1 w/v% aq. P-cell formed white loose fibrous powders (inset, Fig. 3a,c) at high 0.37 g h^{-1} productivity but a low 37.3% yield (Table S1), losing substantially from adhering to the cyclone wall, typical of the lab-scale spray dryer. With increasing KCl loads, the SD P-cell/KCl productivity and yields increased slightly from 0.38 to 0.45 g h^{-1} and 38.3–45.3%, respectively (Table S1). In a closer examination by SEM, SD P-cell powders maintained the fibrillar structure (Fig. 3a,b), while those of P-cell/KCl showed 0.5–2 μm diameter KCl spheres well distributed on fiber surfaces and some associated with smaller fiber fragments likely through charge neutralization of P-cell by K^+ counterions (Fig. 3c,d). Energy-dispersive X-ray spectroscopy (EDS) exhibited prominent C and O peaks that both are typical of cellulose, and a P peak at around 2.02 keV confirms the phosphorous incorporation *via* phosphorylation (Fig. 3e).

The freezing (−80 °C, 15 h) and lyophilization of aqueous (aq.) P-cell produced three-dimensional porous structures (Fig. 4a) in the shape of the conical tube (Fig. S2b) and broke apart easily upon handling by a pair of forceps. The 95.1% yield was due to some loss of fibers adhering to the conical tube walls (Table S1). As expected, similar to spray-dried powders, C, O, and P peaks were observed for FD P-cell (Fig. 4e, 1). P-cell suspensions had the highest electrostatic repulsion, which could minimize the close association among fibers while freeze-drying. With KCl, the presence of K^+ counterions neutralizes electrostatic repulsion among anionic charges on the fiber surfaces to more substantially assembly into more packed and less porous structures with numerous KCl concentrated areas (Fig. 4c,d) and confirmed by EDS analysis (Fig. 4e). FD 1:1 P-cell/KCl could easily be cut into a cylindrical shape without apparent deformation using a sharp razor. FD is a slow process with the lowest productivity of 0.02 g h^{-1}, at least 6 and 18 times lower than OD and SD, respectively (Table S1).

Oven-drying of aqueous P-cell suspensions generated opaque paper-like films (Fig. S2c), in 0.12 mm thickness and relatively macroscopically packed fibers (Fig. 5a) in 95% yield (Table S1). Closer observations by SEM revealed a compact fibrous structure without any observable individual fibers (Fig. 5a). Despite their highest electrostatic repulsion, this well laterally packed and significant interfibrillar association was due to hydrogen bonding during slow oven-drying. The transverse cross-section showed large pieces consisting of multiple bundles with some fibers protruding from the fractured surface and revealing some open porous (Fig. 5b). In contrast, OD 1:1 P-cell/KCl showed numerous large darker grains distributed nonuniformly over its surface, as seen in Fig. 5c. Oven-drying generated 0.12 g h^{-1} with or without KCl and was intermediate to the slow FD and fast SD in productivity. Additionally, the P-cell/KCl yields and thickness (0.14–0.21 mm) increased with KCl loads ranging 96–99% (Table S1). Cross-sectional images of OD 1:1 P-cell showed similar bundles with some individual fibers and open porous ones. Besides, KCl crystal formation resulting from drying was observed among fiber bundles and confirmed by EDS (Fig. 5d), with brighter areas signifying higher KCl concentration (Fig. 5e 2,3). Although the morphological structures produced from these drying methods were consistent with expectations, the charge effect of potassium counterion has not been reported on cellulose fibers functionalized by phosphorylation and, therefore, was further characterized and presented in the following section.

3.3. Characteristics of SD, FD, and OD P-cell/KCl solids

FTIR spectra showed the chemical changes to the P-cell structure following KCl loading and drying methods (Fig. 6a). All of them showed typical P-cell characteristic bands as previously described. The main difference is the more intense band at 1403 cm^{-1} corresponding to the KCl-solvated water (H_2O) (Max and Chapados, 1999) in SD 1:1 P-cell/KCl and FD 1:1 P-cell/KCl. This 1403 cm^{-1} band intensified

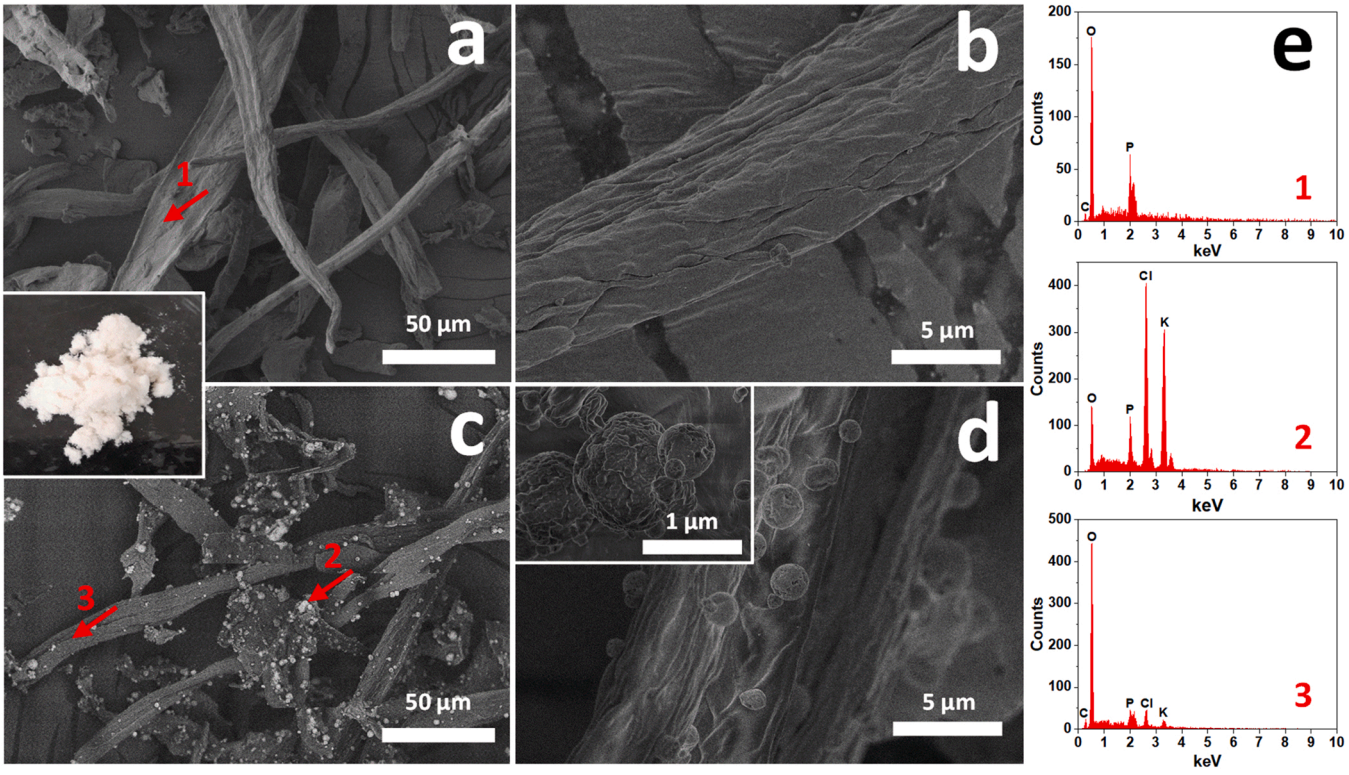

Fig. 3. SEM images of spray-dried (a,b) P-cell and (c,d) 1:1 P-cell/KCl and their (e) EDS spectra. The left inset in (a,c) is a photograph of powders, and the red arrows indicate the sample regions where SEM-EDS conducted the elemental analysis.

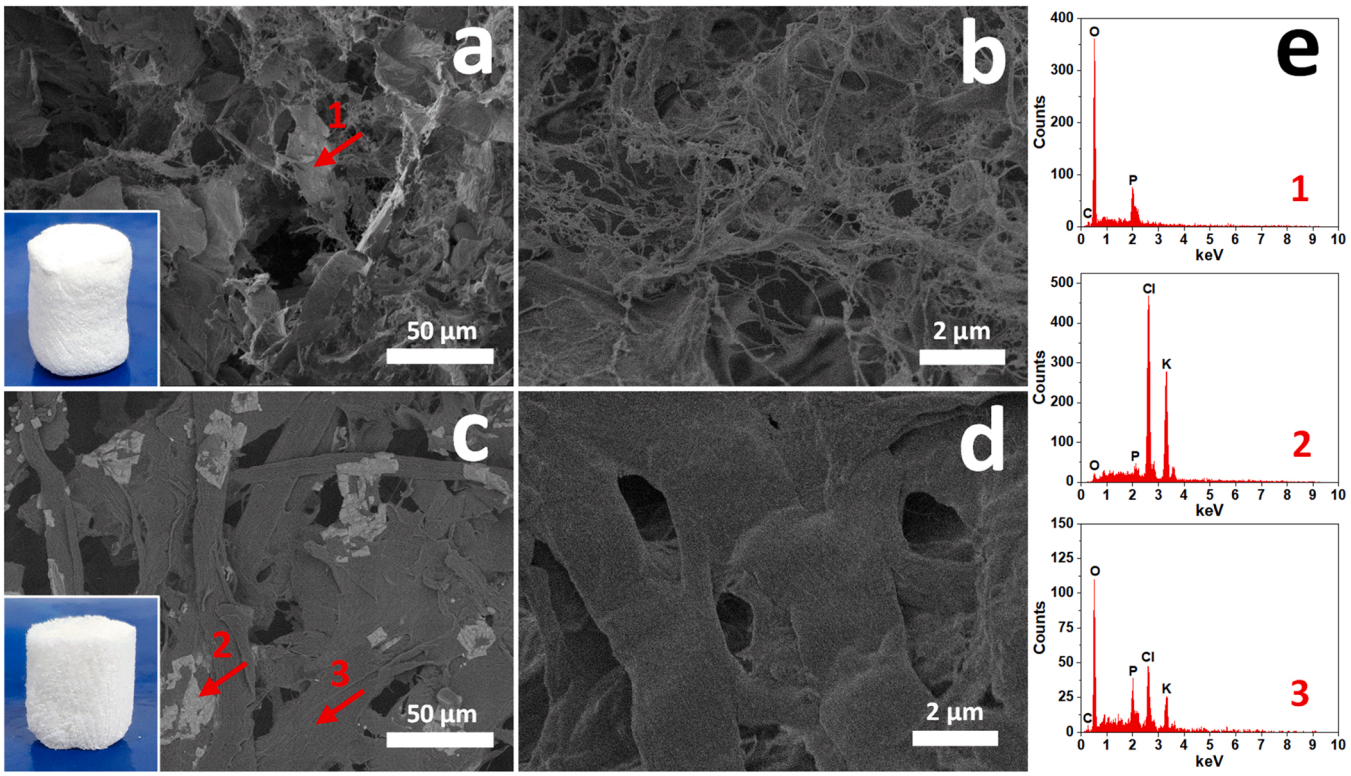

Fig. 4. SEM images of freeze-dried (a,b) P-cell and (c,d) 1:1 P-cell/KCl and their (e) EDS spectra. Left insets in (a,c) are photographs of solids, and the red arrows indicate the sample regions where SEM-EDS analyzed the elemental composition.

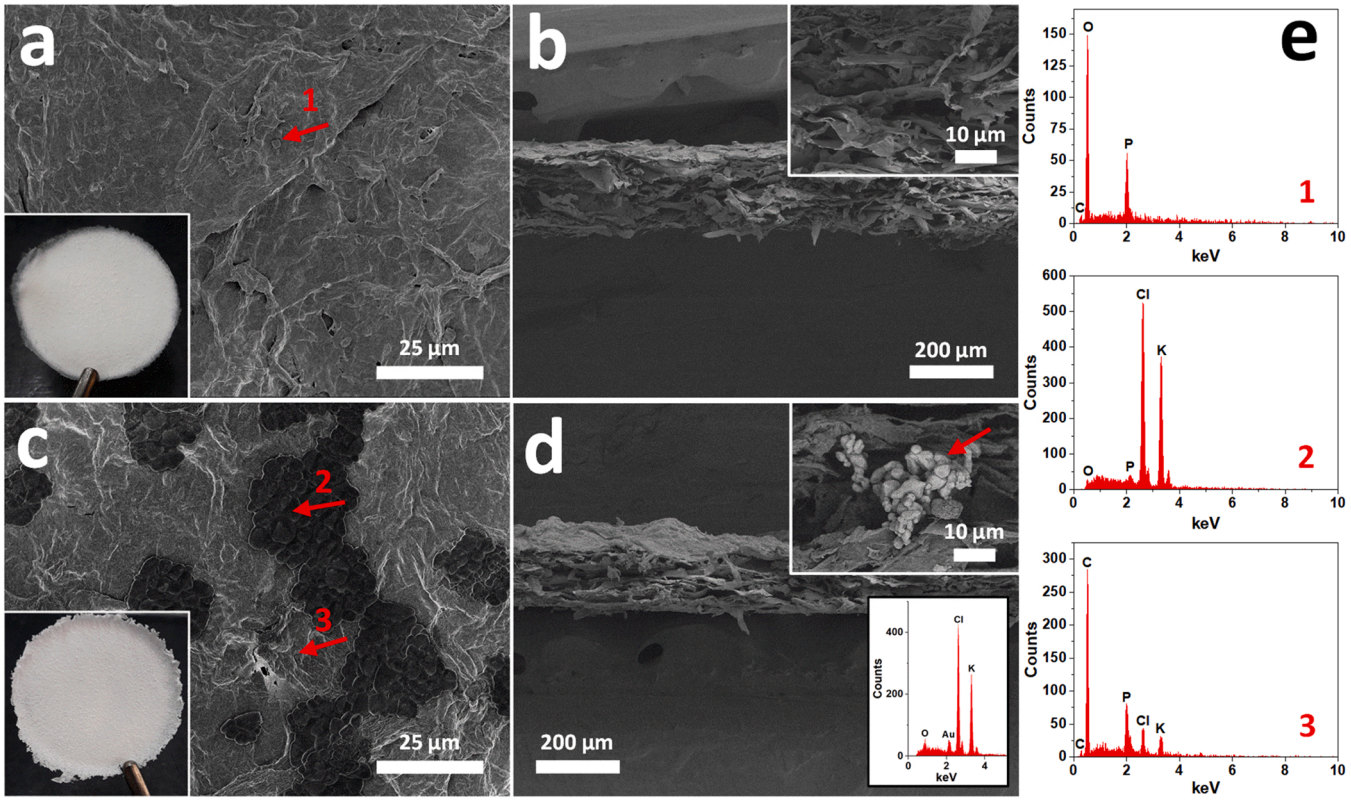

Fig. 5. SEM images of oven-dried (a,b) P-cell and (c,d) 1:1 P-cell/KCl and their (e) EDS spectra: (a,c) top surface and (b,d) transverse cross-sections. The lower left insets in (a,c) are photographs of the films, and the red arrows indicate the sample regions where SEM-EDS analyzed elemental composition.

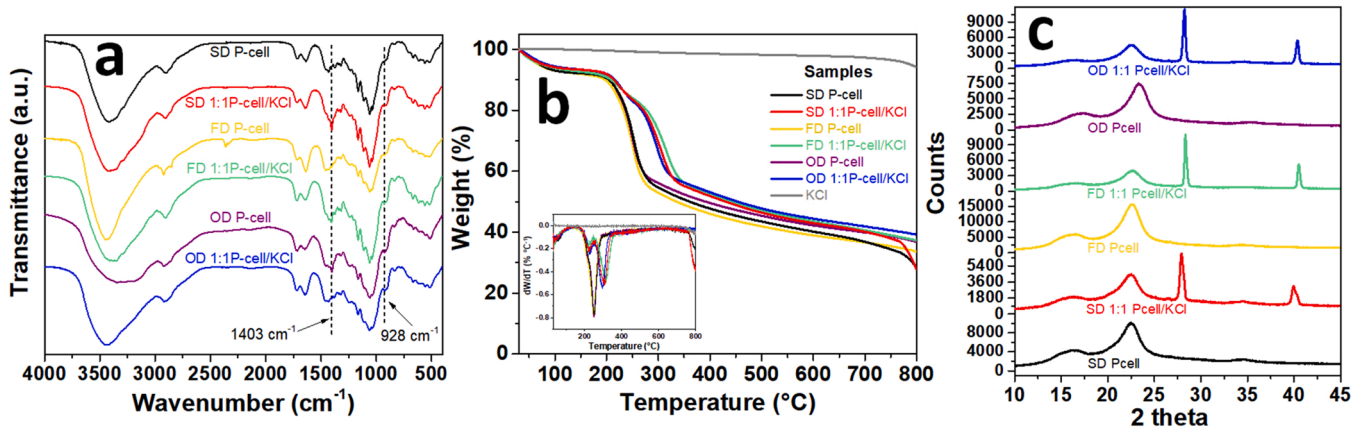

Fig. 6. Characterizations of P-cell and P-cell/KCl dried by the three different drying methods: (a) FTIR spectra, (b) TGA and dTGA curves, and (c) XRD patterns.

with increasing KCl loads for both FD and SD samples from 1:1 P-cell/KCl to 1:4 P-cell/KCl (Fig. S3a), suggesting more potassium loads were exposed on the surface of the sample. In contrast to slow FD and fast SD, the absence of 1403 cm^{-1} for OD 1:1 P-cell/KCl is probably due to the strong aggregation of P-cell fibers in a tight and dense network around the KCl particles, which resulted in no absorbance even under the higher KCl loads (Fig. S3b,c), confirming the potassium loads is covered in this structure. A distinct and slight shoulder at 928 cm^{-1} in all dried P-cell/KCl samples suggests ionic interactions among the anionic phosphate surfaces on P-cell and potassium cations.

Dried P-cell/KCl samples significantly differed in thermal behavior from the dried P-cell ones (Fig. 6b). FD, SD, and OD P-cell exhibited an initial slight mass loss of 8.1–6.6% below 150 °C from water evaporation, followed by one expressive mass loss (*ca.* 40%) from cellulose decomposition. Also, there are slight differences in maximum degradation temperature (249.8–252.1 °C), leaving 38.9–42.2% char residue at 600 °C, possibly due to the distinct hydrogen bonds among P-cell fibers under these three drying methods (Peng et al., 2013b). All KCl-based dried P-cell were less hygroscopic, evaporating 7.3–6.4% moisture and losing about 38% in two stages near 223.6–226.0 °C (T_{max1}) and 297.8–316.1 °C (T_{max2}). This behavior suggests non-simultaneous decomposition of the crystalline cores and the potassium phosphorylates surfaces. The char residues at 600 °C increased with KCl loads, leaving slightly more char residues (43.0–45.5%) than SCB cellulose, which is consistent with the more thermal stable potassium chloride content noticed with only one slight mass loss above 760 °C for pure KCl. In conclusion, the potassium loading influenced the resulting thermal stabilities and char residues left at all three loading levels independent of the drying method used (Fig. S4).

All dried P-cell and P-cell/KCl samples retained the monoclinic Iβ form of cellulose, with typical 2θ peaks at 2θ = 14.8°, 16°6, and 22.6° correspondent to the respective 1 $\bar{1}$ 0, 1 1 0, and 2 0 0 crystallographic planes (Fig. 6c). More intense peaks at 2θ = 28.3° and 40.5° of dried P-cell/KCl samples are attributed to KCl salt crystalline phases (Cong and Cao, 2006). Both peaks' increasing diffraction intensity values with increasing KCl amount (Fig. S5) follow the same trend as their char residues for all P-cell/KCl samples. SD and FD P-cell samples had CrI values of 67% and 71%, respectively, lower than the OD P-cell with 73% CrI, showing lower crystallinity from SD. Similarly, nanofibrillated cellulose generated from softwood bleached pulp *via* mechanical disintegration also led to lower crystalline from spray- (72%) as compared to the oven- (80%) and freeze- (78%) drying (Žepič et al., 2014). In contrast to the slow oven-drying, as the shorter drying time (fast dehydration) from spray-drying may limit the rearrangement of cellulose chains (Peng et al., 2013a), fewer hydrogen bonds among P-cell fibers are expected. Therefore, Freeze-drying is considered to have the least effect on fibrillar structure. The higher CrI value of OD P-cell could result from hydrogen bonding during the gradual dehydration process (8 h), driving P-cell fibers to come closer to each other to possibly inducing inter-fibrillar crystallization. SD, FD, and OD P-cell/KCl samples had CrI values of 66%, 70%, and 70%, respectively, similar to their respective P-cell, signifying their crystallinity did not suffer significant changes after KCl loading (Table 1).

3.4. Release of potassium in water

The release of potassium from SD, FD, and OD P-cell/KCl solids in water was studied. Normalized by weight, SD P-cell/KCl 1:1, 1:2, 1:4 molar ratios lost similar maximums 92.7, 90.4, 97.3% of potassium, respectively (Fig. 7a) and small quantities of fibers (Fig. S6a-d). A rapid release (83.7, 93.6%) occurred within the first 20 min (stage I) followed by another 3.07–6.77% after 168 h (stage II) for SD 1:2 P-cell/KCl and SD 1:4 P-cell/KCl. Most impressively, SD 1:1 P-cell/KCl released potassium at three stages of 76.6% in 20 min (stage I), then slow 2.04% (stage II) in 6 h, and 14.0% (stage III) in 168 h (Fig. 7a). A slower release rate may be linked to stronger electrostatic attraction interactions from the equal anionic/cationic loadings between cellulose anionic phosphate groups and potassium ions.

In the case of all three-dimensional porous FD structures, a full release of 73.5, 78.4, 81.7% potassium (Fig. 7b), slower than SD P-cell/KCl (92.7, 90.4, 97.3%) over the same period, indicating potassium release to be dependent of the assembled solid structure of fibers. Furthermore, FD 1:1 P-cell/KCl, 1:2 P-cell/KCl, and 1:4 P-cell/KCl showed great physical integrity in the water while FD P-cell fell (Fig. S6e-f). At the same equal anionic/cationic loading, FD 1:1 Pcell/KCl released potassium at three stages of 57.7% in 20 min (stage I), then 3.78% in 6 h (stage II), and lastly, 15.7% in 168 h (stage III) as the SD counterpart (Fig. 7b). In contrast, those FD 1:2 P-cell/KCl and FD 1:4 P-cell/KCl released 69.8% and 74.1% potassium in 5 min (stage I),

Table 1
Comparison of drying time, crystalline and thermal properties of P-cell and P-cell/KCl solids. SD spray-drying, FD freeze-drying, OD oven-drying, ND: no data.

Sample	Drying time	CrI (%)	Moisture loss at 150 °C (-%)	T_{max1} (°C)	T_{max2} (°C)	Chair at 600 °C (%)
SD P-cell	1 h	67	7.8	250.5	ND	40.2
SD 1:1 P-cell/KCl		66	6.6	225.6	306.5	43.0
FD P-cell	2 d	71	8.1	249.8	ND	38.9
FD 1:1 P-cell/KCl		70	7.3	223.6	316.1	43.6
OD P-cell	8 h	73	6.6	252.1	ND	42.2
OD 1:1 P-cell/KCl		70	6.4	226.0	297.8	45.5

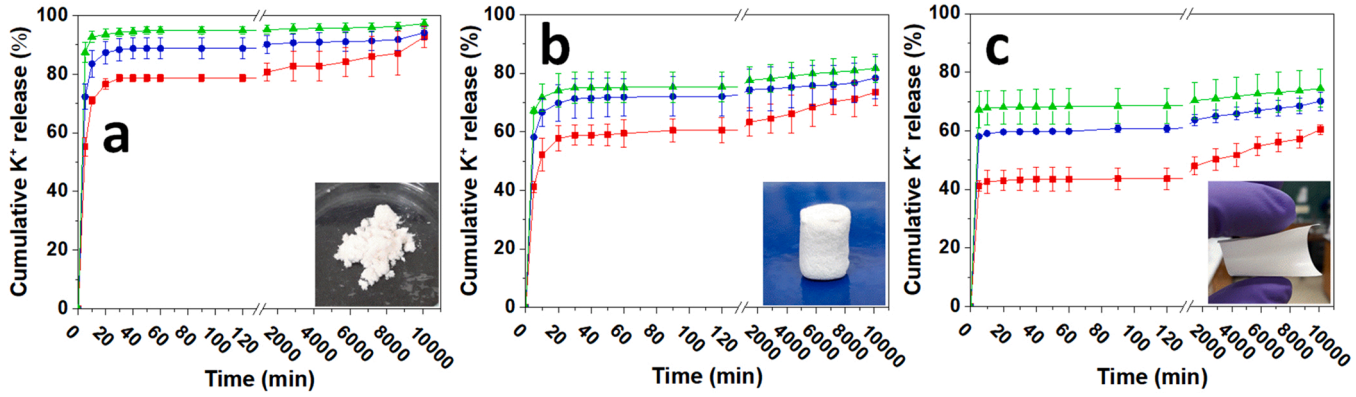

Fig. 7. Cumulative release of potassium in water from (a) SD, (b) FD, and (c) OD solids with 1:1 P-cell/KCl (red), 1:2 P-cell/KCl (blue), and 1:4 P-cell/KCl (green) compositions.

followed by a much smaller release of 7.6, 8.6% in 168 h (stage II).

Most impressively, the highly compacted OD 1:1, 1:2, and 1:4 Pcell/KCl paper-like films released 60.4, 69.2, 74.5% potassium, substantially slower than those from FD and SD series, even though none of OD exhibited any observable change in their physical integrity in water for one week (Fig. S6g-h). All films released potassium in three stages even under the higher anionic/cationic loading, showing a reduced burst release of 41.2, 58.1, 67.2% potassium within 5–10 min (stage I), followed by a slow one of 3.58%, 2.2%, and 1.7% after 6–7 h, and lastly an expressive release of 15.65%, 8.9%, and 5.6% from OD 1:1 P-cell/KCl, OD 1:2 P-cell/KCl, and OD 1:4 Pcell/KCl, respectively (Fig. 7c). These brief initial periods of potassium release from paper-like films were 2–4 times shorter than those solids from SD and FD. Overall, the lowest potassium rate released is associated with increasing compaction levels of the assembled fibrillar structures, *i.e.*, 32% and 14% potassium released more quickly from SD 1:1 P-cell/KCl and FD 1:1 P-cell/KCl compared to the OD 1:1 P-cell/KCl. Since anionic phosphoric groups on P-cell cannot electrostatically bind the excess K^+ cations, K^+ to Cell-O-HPO_3^- molar ratios higher than equal cationic/anionic loading are related to the faster potassium release rates, independent of the drying method.

The morphological structure and potassium release data provide direct evidence that the formation of highly compacted structure from slow oven-drying lead to fewer potassium loads exposed to release and improves slowing release. Besides, the equal cationic/anionic loading was also more effective in promoting a slowing release driven by stronger attractive electrostatic forces, even though dried into different solid structures by the three dryings.

Cumulative release of K from FD 1:1 P-cell/KCl, OD 1:1 P-cell/KCl, and OD 1:2 P-cell/KCl fitted the Korsmeyer-Peppas model well and correlated coefficients (R^2) varying from 0.9932 to 0.9991 (Fig. 8a, b).

Table 2
Korsmeyer-Peppas kinetic model parameters of first 60% of potassium release and in water from P-cell/KCl solids. ND: no data.

Sample	Release stage	Time (h)	Cumulative Release (%)	Release exponent, *n*	Correlation coefficient, R^2
SD 1:1 P-cell/KCl	I	0.33	76.6	ND	ND
	II	7	2.04		
	III	168	14.0		
SD 1:2 P-cell/KCl	I	0.33	83.7	ND	ND
	II	168	6.77		
SD 1:4 P-cell/KCl	I	0.33	93.6	ND	ND
	II	168	3.70		
FD 1:1 P-cell/KCl	I	0.33	57.7	0.025	0.9982
	II	7	3.78		
	III	168	15.65		
FD 1:2 P-cell/KCl	I	0.33	69.8	ND	ND
	II	168	8.6		
FD 1:4 P-cell/KCl	I	0.33	74.1	ND	ND
	II	168	7.6		
OD 1:1 P-cell/KCl	I	0.08	41.2	0.053	0.9932
	II	6	3.8		
	III	168	15.7		
OD 1:2 P-cell/KCl	I	0.17	58.1	0.025	0.9991
	II	6	2.2		
	III	168	8.9		
OD 1:4 P-cell/KCl	I	0.08	67.2	ND	ND
	II	7	1.7		
	III	168	5.6		

The samples had a release exponent (*n*) lower than 0.5 (Table 2) for the first 60% of potassium released, corresponding to the quasi-Fickian diffusion mechanism. Therefore, the above results support that K^+

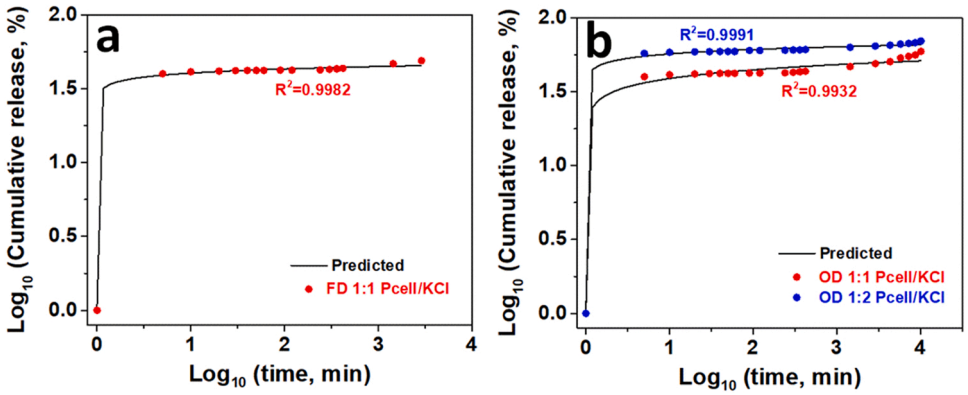

Fig. 8. Model-fitting of Korsmeyer-Peppas of potassium release and in water from (a) freeze- and (b) oven-dried P-cell/KCl solids.

diffuses through swollen and negatively charged FD and OD P-cell/KCl. This slowed potassium release driven by attractive electrostatic forces may be extended to other macro and micronutrients in their cationic form (NH_4^+, Mg^{2+}, Ca^{2+}, Fe^{2+}, Zn^{2+}, Mn^{2+}, Cu^{2+}, *etc.*), providing more diverse applications within the fertilizer-release field. Enhanced efficiency fertilizers from these diverse phosphorylated cellulose fibers substrates offer a prolonged release of potassium. Their simple development approach without requiring extra chemicals or several steps adds economic benefits to the production costs. This work shows the versatility of P-cell fibers to be engineered into different structures for potassium release. It represents the most systematic and optimized approach to tunable their solid form from drying and phosphoric surface chemistry, reported for the first time to our knowledge.

4. Conclusion

The powder-like fibrous, paper-like films and three-dimensional porous structures have been facilely fabricated from their aqueous phosphorylated cellulose fibers suspensions to exhibit tunable release capability behavior. $(NH_4)_2HPO_4$ phosphorylation of cellulose yielded long fibers (14.6 μm wide, *ca.* 366 μm length), slightly more crystalline (72%) than SCB cellulose (69%), and with newly introduced phosphate groups on its surface (2.4 mmol g^{-1} charges). The rapid spray-drying of charged P-cell fibers suspensions generated fibrous morphology powders at lower yields of 37%. With increasing KCl loads, P-cell/KCl powders had up to 45% yields, while their morphology was not significantly affected by the neutralization of surface charge repulsion effects. Soft and porous solids with three-dimensional structures were assembled from freeze-drying of P-cell aqueous suspensions, showing 13.3 μm width and higher 95–97% yields. Due to surface charge neutralizing induced by potassium cation, P-cell/KCl suspensions could be more robustly assembled into thinnest (11.6 μm width) and less apparent porosity structures. Oven-drying, on the other hand, compacted P-cell fibers at 95–99% yields and induced inter-fibers crystallization (73%) into opaque and more thermally stable (252.1 °C) films than the spray-dried (67%, 250.5 °C) and freeze-dried counterparts (71%, 249.8 °C). Potassium counterion bound to P-cell fiber solids exhibited structure solid dependent release followed by a quasi-Fickian diffusion mechanism in water. This work demonstrates a facile and feasible strategy to explore phosphorylated cellulose fibers derived from the sugarcane bagasse as solid substrates to chemically bind and control the release of potassium cations for the first time to our knowledge.

CRediT authorship contribution statement

Lucas Luiz Messa: Investigation, Formal analysis, Funding acquisition, Methodology, Data curation, Writing – original draft, Writing – review & editing. **You-Lo Hsieh**: Conceptualization, Supervision, Writing – review & editing. **Roselena Faez**: Conceptualization, Supervision, Funding acquisition, Writing – review & editing.

Declaration of Competing Interest

The authors declare that they have no known competing financial interests or personal relationships that could have appeared to influence the work reported in this paper.

Data availability

Data will be made available on request.

Acknowledgments

The authors are grateful to Sao Paulo Research Foundation - FAPESP-Brazil (2017/03980-7, 2019/08057-8 and 2019/02535-5) and Coordenação de Aperfeiçoamento de Pessoal de Nível Superior - Brazil (CAPES) - Finance Code 001 for financial support. R.F. is a CNPq researcher.

Appendix A. Supporting information

Supplementary data associated with this article can be found in the online version at doi:10.1016/j.indcrop.2022.115350.

References

Abushammala, H., Mao, J., 2019. A review of the surface modification of cellulose and nanocellulose using aliphatic and aromatic mono- and di-isocyanates. Molecules 24, 1–18. https://doi.org/10.3390/molecules24152782.

Aoki, D., Nishio, Y., 2010. Phosphorylated cellulose propionate derivatives as thermoplastic flame resistant/retardant materials: influence of regioselective phosphorylation on their thermal degradation behaviour. Cellulose 17, 963–976. https://doi.org/10.1007/s10570-010-9440-8.

Ardanuy, M., Claramunt, J., Toledo Filho, R.D., 2015. Cellulosic fiber reinforced cement-based composites: a review of recent research. Constr. Build. Mater. 79, 115–128. https://doi.org/10.1016/j.conbuildmat.2015.01.035.

Bortolin, A., Aouada, F.A., Mattoso, L.H.C., Ribeiro, C., 2013. Nanocomposite PAAm/methyl cellulose/montmorillonite hydrogel: evidence of synergistic effects for the slow release of fertilizers. J. Agric. Food Chem. 61, 7431–7439. https://doi.org/10.1021/jf401273n.

Chen, J., Lü, S., Zhang, Z., Zhao, X., Li, X., Ning, P., Liu, M., 2018. Environmentally friendly fertilizers: a review of materials used and their effects on the environment. Sci. Total Environ. 613–614, 829–839. https://doi.org/10.1016/j.scitotenv.2017.09.186.

Cichosz, S., Masek, A., 2019. Cellulose structure and property changes indicated via wetting-drying cycles. Polym. Degrad. Stab. 167, 33–43. https://doi.org/10.1016/j.polymdegradstab.2019.05.033.

Cong, H., Cao, W., 2006. Preparation of ordered porous NaCl and KCl crystals. Solid State Sci. 8, 1056–1060. https://doi.org/10.1016/j.solidstatesciences.2005.12.012.

FAOSTAT, 2020. Food and Agricultural Organization of United Nations: Economic and Social Department: The Statistical Division [WWW Document]. URL http://www.fao.org/faostat/en/#data/QC (accessed 10.15.21).

Ferreira-Leitao, V., Gottschalk, L.M.F., Ferrara, M.A., Nepomuceno, A.L., Molinari, H.B. C., Bon, E.P.S., 2010. Biomass residues in Brazil: availability and potential uses. Waste Biomass Valoriz. 1, 65–76. https://doi.org/10.1007/s12649-010-9008-8.

Ghanadpour, M., Carosio, F., Larsson, P.T., Wågberg, L., 2015. Phosphorylated cellulose nanofibrils: a renewable nanomaterial for the preparation of intrinsically flame-retardant materials. Biomacromolecules 16, 3399–3410. https://doi.org/10.1021/acs.biomac.5b01117.

Ghanadpour, M., Carosio, F., Ruda, M.C., Wågberg, L., 2018a. Tuning the nanoscale properties of phosphorylated cellulose nanofibril-based thin films to achieve highly fire-protecting coatings for flammable solid materials. ACS Appl. Mater. Interfaces 10, 32543–32555. https://doi.org/10.1021/acsami.8b10309.

Ghanadpour, M., Wicklein, B., Carosio, F., Wågberg, L., 2018b. All-natural and highly flame-resistant freeze-cast foams based on phosphorylated cellulose nanofibrils. Nanoscale 10, 4085–4095. https://doi.org/10.1039/c7nr09243a.

Jiang, F., Han, S., Hsieh, Y.Lo, 2013. Controlled defibrillation of rice straw cellulose and self-assembly of cellulose nanofibrils into highly crystalline fibrous materials. RSC Adv. 3, 12366–12375. https://doi.org/10.1039/c3ra41646a.

Kafkafi, U., Xu, G., Imas, P., Magen, H., Tarchitzky, J., Johnston, A., 2001. Potassium and chloride in crops and soils: the role of potassium chloride fertilizer in crop nutrition. Int. Potash Inst. 220.

Kenawy, E.R., Azaam, M.M., El-nshar, E.M., 2018. Preparation of carboxymethyl cellulose-g-poly (acrylamide)/montmorillonite superabsorbent composite as a slow-release urea fertilizer. Polym. Adv. Technol. 29, 2072–2079. https://doi.org/10.1002/pat.4315.

Kim, J., Yun, S., Ounaies, Z., 2006. Discovery of cellulose as a smart material. Macromolecules 39, 4202–4206. https://doi.org/10.1021/ma060261e.

Korovnikova, N., Dubyna, O., Oliinik, V., Svishchova, Y., 2020. Chemical cellulose-based fibers of decreased flammability. East. Eur. J. Enterp. Technol. 5, 33–39. https://doi.org/10.15587/1729-4061.2020.214507.

Korsmeyer, R.W., Gurny, R., Doelker, E., Buri, P., Peppas, N.A., 1983. Mechanisms of solute release from porous hydrophilic polymers. Int. J. Pharm. 15, 25–35. https://doi.org/10.1016/0378-5173(83)90064-9.

Kumar, A., Singh Negi, Y., Choudhary, V., Bhardwaj, N.K., 2014. Characterization of cellulose nanocrystals produced by acid-hydrolysis from sugarcane bagasse as agro-waste; characterization of cellulose nanocrystals produced by acid-hydrolysis from sugarcane bagasse as agro-waste. J. Mater. Phys. Chem. 2, 1–8. https://doi.org/10.12691/jmpc-2-1-1.

Lehtonen, J., Hassinen, J., Kumar, A.A., Johansson, L.S., Mäenpää, R., Pahimanolis, N., Pradeep, T., Ikkala, O., Rojas, O.J., 2020. Phosphorylated cellulose nanofibers exhibit exceptional capacity for uranium capture. Cellulose 8. https://doi.org/10.1007/s10570-020-02971-8.

Li, K., Wang, J., Liu, X., Xiong, X., Liu, H., 2012. Biomimetic growth of hydroxyapatite on phosphorylated electrospun cellulose nanofibers. Carbohydr. Polym. 90, 1573–1581. https://doi.org/10.1016/j.carbpol.2012.07.033.

Li, X., Li, Q., Su, Yuan, Yue, Q., Gao, B., Su, Yi, 2015. A novel wheat straw cellulose-based semi-IPNs superabsorbent with integration of water-retaining and controlled-

release fertilizers. J. Taiwan Inst. Chem. Eng. 55, 170–179. https://doi.org/10.1016/j.jtice.2015.04.022.
Li, Y., Zhen, D., Liao, S., Zhu, D., Yang, X., 2018. Controlled-release urea encapsulated by ethyl cellulose/butyl acrylate/vinyl acetate hybrid latex. Pol. J. Chem. Technol. 20, 108–112. https://doi.org/10.2478/pjct-2018-0062.
Liu, P., Borrell, P.F., Božič, M., Kokol, V., Oksman, K., Mathew, A.P., 2015. Nanocelluloses and their phosphorylated derivatives for selective adsorption of Ag+, Cu2+ and Fe3+ from industrial effluents. J. Hazard. Mater. 294, 177–185. https://doi.org/10.1016/j.jhazmat.2015.04.001.
Mandal, A., Chakrabarty, D., 2011. Isolation of nanocellulose from waste sugarcane bagasse (SCB) and its characterization. Carbohydr. Polym. 86, 1291–1299. https://doi.org/10.1016/j.carbpol.2011.06.030.
Mautner, A., Maples, H.A., Kobkeatthawin, T., Kokol, V., Karim, Z., Li, K., Bismarck, A., 2016. Phosphorylated nanocellulose papers for copper adsorption from aqueous solutions. Int. J. Environ. Sci. Technol. 13, 1861–1872. https://doi.org/10.1007/s13762-016-1026-z.
Max, J.J., Chapados, C., 1999. Interpolation and extrapolation of infrared spectra of binary ionic aqueous solutions. Appl. Spectrosc. 53, 1601–1609. https://doi.org/10.1366/0003702991946064.
Messa, L.L., Faez, R., Hsieh, Y., 2021. Phosphorylated cellulose nanofibrils from sugarcane bagasse with pH tunable gelation. Carbohydr. Polym. Technol. Appl. 2, 100085 https://doi.org/10.1016/j.carpta.2021.100085.
Mohammadi-Khoo, S., Moghadam, P.N., Fareghi, A.R., Movagharnezhad, N., 2016. Synthesis of a cellulose-based hydrogel network: characterization and study of urea fertilizer slow release. J. Appl. Polym. Sci. 133, 1–9. https://doi.org/10.1002/app.42935.
Muharam, S., Fitri, A., Yuningsih, L.M., Putri, Y.M.T.A., Rahmawati, I., 2020. Synthesis and characterization of controlled-release urea fertilizer from superabsorbent hydrogels. Indones. J. Chem. https://doi.org/10.22146/ijc.44230.
Naderi, A., Lindström, T., Weise, C.F., Flodberg, G., Sundström, J., Junel, K., Erlandsson, J., Runebjörk, A.M., 2016. Phosphorylated nanofibrillated cellulose: production and properties. Nord. Pulp Pap. Res. J. 31, 20–29. https://doi.org/10.3183/npprj-2016-31-01-p020-029.
Nardi, R., Silveira, M.H.L., Siqueira, G., 2020. Understanding important aspects of spray drying microfibrillated cellulose through statistical analysis. Cellulose 27, 10707–10717. https://doi.org/10.1007/s10570-020-03392-3.
Niu, F., Wu, N., Yu, J., Ma, X., 2020. Gelation, flame retardancy, and physical properties of phosphorylated microcrystalline cellulose aerogels. Carbohydr. Polym. 242, 116422 https://doi.org/10.1016/j.carbpol.2020.116422.
Noguchi, Y., Homma, I., Matsubara, Y., 2017. Complete nanofibrillation of cellulose prepared by phosphorylation. Cellulose 24, 1295–1305. https://doi.org/10.1007/s10570-017-1191-3.
Olad, A., Zebhi, H., Salari, D., Mirmohseni, A., Reyhani Tabar, A., 2018. Slow-release NPK fertilizer encapsulated by carboxymethyl cellulose-based nanocomposite with the function of water retention in soil. Mater. Sci. Eng. C 90, 333–340. https://doi.org/10.1016/j.msec.2018.04.083.
Peng, Y., Gardner, D.J., Han, Y., Cai, Z., Tshabalala, M.A., 2013a. Influence of drying method on the surface energy of cellulose nanofibrils determined by inverse gas chromatography. J. Colloid Interface Sci. 405, 85–95. https://doi.org/10.1016/j.jcis.2013.05.033.
Peng, Y., Gardner, D.J., Han, Y., Kiziltas, A., Cai, Z., Tshabalala, M.A., 2013b. Influence of drying method on the material properties of nanocellulose I: thermostability and crystallinity. Cellulose 20, 2379–2392. https://doi.org/10.1007/s10570-013-0019-z.
Rocha, G.J. de M., Nascimento, V.M., Gonçalves, A.R., Silva, V.F.N., Martín, C., 2015. Influence of mixed sugarcane bagasse samples evaluated by elemental and physical-chemical composition. Ind. Crop. Prod. 64, 52–58. https://doi.org/10.1016/j.indcrop.2014.11.003.
Rol, F., Naceur, M., Gandini, A., Bras, J., 2019a. Recent advances in surface-modified cellulose nanofibrils. Prog. Polym. Sci. 88, 241–264. https://doi.org/10.1016/j.progpolymsci.2018.09.002.
Rol, F., Sillard, C., Bardet, M., Yarava, J.R., Emsley, L., Gablin, C., Léonard, D., Belgacem, N., Bras, J., 2019b. Cellulose phosphorylation comparison and analysis of phosphorate position on cellulose fibers. Carbohydr. Polym. 229, 115294 https://doi.org/10.1016/j.carbpol.2019.115294.
Rop, K., Karuku, G.N., Mbui, D., Michira, I., Njomo, N., 2018. Formulation of slow release NPK fertilizer (cellulose-graft-poly(acrylamide)/nano-hydroxyapatite/soluble fertilizer) composite and evaluating its N mineralization potential. Ann. Agric. Sci. 63, 163–172. https://doi.org/10.1016/j.aoas.2018.11.001.
Saxena, I.M., Brown, R.M., 2005. Cellulose biosynthesis: current views and evolving concepts. Ann. Bot. 96, 9–21. https://doi.org/10.1093/aob/mci155.
Segal, L., Creely, J.J., Martin, A.E., Conrad, C.M., 1959. An empirical method for estimating the degree of crystallinity of native cellulose using the X-ray diffractometer. Text. Res. J. 29, 786–794. https://doi.org/10.1177/004051755902901003.
Senna, A.M., Braga Do Carmo, J., Santana Da Silva, J.M., Botaro, V.R., 2015. Synthesis, characterization and application of hydrogel derived from cellulose acetate as a substrate for slow-release NPK fertilizer and water retention in soil. J. Environ. Chem. Eng. 3, 996–1002. https://doi.org/10.1016/j.jece.2015.03.008.
Shi, Y., Belosinschi, D., Brouillette, F., Belfkira, A., Chabot, B., 2015. The properties of phosphorylated kraft fibers. BioResources 10, 4375–4390. https://doi.org/10.15376/biores.10.3.4375-4390.
Suflet, D.M., Chitanu, G.C., Popa, V.I., 2006. Phosphorylation of polysaccharides: new results on synthesis and characterisation of phosphorylated cellulose. React. Funct. Polym. 66, 1240–1249. https://doi.org/10.1016/j.reactfunctpolym.2006.03.006.
Vikman, M., Vartiainen, J., Tsitko, I., Korhonen, P., 2015. Biodegradability and compostability of nanofibrillar cellulose-based products. J. Polym. Environ. 23, 206–215. https://doi.org/10.1007/s10924-014-0694-3.
Vuoti, S., Laatikainen, E., Heikkinen, H., Johansson, L.S., Saharinen, E., Retulainen, E., 2013. Chemical modification of cellulosic fibers for better convertibility in packaging applications. Carbohydr. Polym. 96, 549–559. https://doi.org/10.1016/j.carbpol.2012.07.053.
Wulandari, W.T., Rochliadi, A., Arcana, I.M., 2016. Nanocellulose prepared by acid hydrolysis of isolated cellulose from sugarcane bagasse. IOP Conf. Ser. Mater. Sci. Eng. 107. https://doi.org/10.1088/1757-899X/107/1/012045.
Žepič, V., Fabjan, E., Kasunič, M., Korošec, R.C., Hančič, A., Oven, P., Perše, L.S., Poljanšek, I., 2014. Morphological, thermal, and structural aspects of dried and redispersed nanofibrillated cellulose (NFC). Holzforschung 68, 657–667. https://doi.org/10.1515/hf-2013-0132.
Zhang, M., Yang, J., 2020. Preparation and characterization of multifunctional slow release fertilizer coated with cellulose derivatives. Int. J. Polym. Mater. Polym. Biomater. 0, 1–8. https://doi.org/10.1080/00914037.2020.1765352.
Zhang, X., Liu, Y., Lu, P., Zhang, M., 2020. Preparation and properties of hydrogel based on sawdust cellulose for environmentally friendly slow release fertilizers. Green Process. Synth. https://doi.org/10.1515/gps-2020-0015.